

RSC Advances



This is an *Accepted Manuscript*, which has been through the Royal Society of Chemistry peer review process and has been accepted for publication.

Accepted Manuscripts are published online shortly after acceptance, before technical editing, formatting and proof reading. Using this free service, authors can make their results available to the community, in citable form, before we publish the edited article. This *Accepted Manuscript* will be replaced by the edited, formatted and paginated article as soon as this is available.

You can find more information about *Accepted Manuscripts* in the [Information for Authors](#).

Please note that technical editing may introduce minor changes to the text and/or graphics, which may alter content. The journal's standard [Terms & Conditions](#) and the [Ethical guidelines](#) still apply. In no event shall the Royal Society of Chemistry be held responsible for any errors or omissions in this *Accepted Manuscript* or any consequences arising from the use of any information it contains.



Fast Diffusion Supercapacitors via Ultra-high Pore Volume of Crumpled 3D Structure Reduced Graphene Oxides Activation

Keunsiik Lee,^{ab} Doyoung Kim,^{ac} Yeoheung Yoon,^a Junghee Yang,^b Ho-Gyeong Yun,^d In-Kyu You^d and Hyoyoung Lee^{*abc}

Received 00th January 20xx,
Accepted 00th January 20xx

DOI: 10.1039/x0xx00000x

www.rsc.org/advances

In order to obtain a high performance supercapacitor, there are several factors that must be achieved including high specific surface area (SSA), high electrical conductivity, and high diffusion rate of the electrolyte due to an appropriate pore volume. Herein, we report a high performance supercapacitor using activated non-stacked reduced graphene oxide (a-NSrGO) that has a high SSA (up to 999.75 m² g⁻¹) with intrinsic high graphene conductivity (1202 S m⁻¹) and a fast diffusion of the electrolyte. Due to the high total pore volume (5.03 cm³ g⁻¹) and wide pore size distribution from macro- to micropores (main pore width: 0.61 - 0.71 nm) in the a-NSrGO sheets, the as-prepared a-NSrGO electrode shows high specific capacitance (105.26 F g⁻¹) and short relaxation time ($\tau_0 = 1.5$ s) in a propylene carbonate (PC)-based organic electrolyte. The maximum energy density of 91.13 Wh kg⁻¹ and power density of 66684.73 W kg⁻¹ were estimated in full packaged coin cell. The high performance of the a-NSrGO supercapacitors is attributed to their specific appearance and enlarged pore distribution with high SSA.

1. Introduction

Graphene, a 2D sp²-hybridized carbon sheet with one atom thickness, has attracted increasing attention because of its unique structure and properties.^{1, 2} Furthermore, chemically-exfoliated graphene made via Hummer's method, i.e., graphene oxide (GO), can be produced in large quantities. GO, which contains oxygen groups, is a non-conductive material due to its lack of double bonds that possess conjugated pi electrons; however, reduced graphene oxide (rGO), which can be made by thermal reduction or chemical reduction using hydriodic acid (HI),³ has an enhanced high electrical conductivity. Its high theoretical surface area (2630 m² g⁻¹) and high electrical conductivity make it particularly attractive as a material for energy storage systems.^{4, 5} These properties suggest that graphene can be used to replace existing materials, including activated carbons that are non-conductive, in conventional applications such as supercapacitors.⁶ Thus, the use of conductive rGO flakes is expected to be useful in commercially available supercapacitors.

Supercapacitors (or ultracapacitors) that form a double layer of electrolyte ions on the surface of conductive electrodes are considered to be a main contender for energy storage due to their high power performance, long life cycles, and low maintenance costs.^{7, 8} Graphene is an obvious material choice for this application due its high surface area and high conductivity. Currently, graphene-based electrochemical double layer capacitor (EDLC) prototypes lead the field in capacitance, energy density, and power density because of their high electrical conductivity, accessible and defined pore structure, and low equivalent series resistance (ESR).⁴ However, although numerous studies have detailed the use of graphene nanosheets in supercapacitors, real device applications⁹ that are scalable are still in progress; many obstacles remain that still need to be overcome. To enhance the capacitive effect for a supercapacitor, several factors, including the electrical conductivity and specific surface area (SSA), have been considered. The use of graphene flakes is contrary to the use of the bulk amorphous sp³ carbon materials (e.g., activated carbons (ACs)), even when these materials have a high SSA.¹⁰ Therefore, a solution is required to provide materials with both high SSA and high electrical conductivity. In spite of efforts to increase the SSA of graphene flakes, however, there are still problems such as re-stacking or aggregation of the graphene flakes. To avoid these problems, composite materials with graphene flakes have been used to generate pseudo-capacitance causing redox reaction. However, these materials lack capacitance retention and have a low rate performance due to their demand for a redox reaction.

^a Centre for Integrated Nanostructure Physics (CINAP), Institute of Basic Science (IBS), Sungkyunkwan University, 2066 Seoburo, Jangan-gu, Suwon 440-746, Republic of Korea.

^b Department of Chemistry, Sungkyunkwan University, 2066 Seoburo, Jangan-gu, Suwon 440-746, Republic of Korea.

^c Department of Energy Science, Sungkyunkwan University, 2066 Seoburo, Jangan-gu, Suwon 440-746, Republic of Korea.

^d Information & Communications Core Technology Research Laboratory, Electronics and Telecommunication Research Institute (ETRI), Daejeon 305-700, Republic of Korea.

† Electronic Supplementary Information (ESI) available: Detailed experimental methods, figures relating to the characterization of used GO, NSrGO, and a-NSrGO with electrochemical properties. See DOI: 10.1039/x0xx00000x

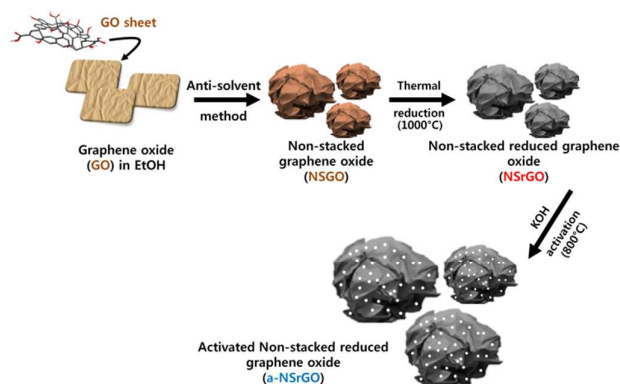


Fig. 1 The schematic illustration of the fabrication a-NSrGO. The graphene oxide (GO) is synthesized by a modified Hummer's method. The non-stacked graphene oxide (NSGO) is prepared from a GO dispersion solution in ethanol (1 mg mL^{-1}) via the anti-solvent method using ethanol and hexane. The NSGO is then reduced by thermal reduction at $1,000^\circ\text{C}$. Finally the a-NSrGO is fabricated by facile KOH activation at 800°C . After activation, the sample is washed with pure water to remove any remaining KOH until the pH reaches 7.

Recently, controlling the pore volume of graphene supercapacitor electrodes has been one of the most effective and efficient factors for enabling fast charging/discharging diffusion performance in supercapacitors, which utilize narrowly controlled sub-nanopores.^{11–13} For example, materials with only high SSA and no control over the pore distribution are not suitable for EDLC supercapacitors, which require fast charging and discharging via fast diffusion pathways for the electrolyte. However, until now, although graphene flakes activated with KOH have been known to give high SSA, the failure to control the pore volume of the 3D graphene electrodes has yielded materials that are insufficient, especially for EDLC supercapacitors. Therefore, in order to obtain good EDLC supercapacitors, a material must have high SSA and electrical conductivity while also maintaining a high pore volume in the 3D graphene flake electrodes in order to allow the electrolyte to diffuse easily.

To solve the critical problems facing EDLC supercapacitors, we report on activated non-stacked reduced graphene oxide (a-NSrGO) electrodes that have high conductivity and high SSA with a wide pore distribution (from macro- to micro-pores) for the best-fit energy storage performance. These materials have been carefully designed to introduce the non-stacked rGO 3D nanostructure (to maintain high pore volume and high SSA) and also to introduce KOH-etching of the graphene flakes (to give high SSA and many diffusion pathways for the electrolyte). The strategy for the synthesis of a-NSrGO is described in Fig. 1. First, we synthesized graphene oxide (GO) by a modified Hummer's method. Then, the non-stacked graphene oxide (NSGO) was prepared via an anti-solvent method using ethanol and hexane, which we developed previously.¹⁴ Briefly, the GO sheets were dispersed in ethanol (1 mg mL^{-1}) to allow the GOs to be fully exfoliated through

strong homogenization. After pouring the non-polar hexane solvent, the resulting precipitates of non-stacked GO (NSGO) sheets were fully dried using a rotary evaporator. The NSGO was then reduced to make NSrGO through a conventional thermal reduction process. To make a-NSrGO, the NSrGO was then placed in a 7 M KOH solution, followed by filtration and drying. The resulting mixture was put in a tube furnace under the flow of an inert gas at 100 sccm and heated at 800°C for 1 h. Finally, the a-NSrGO was obtained after washing unreacted KOH, many type of salt and metal ion with pure water until the pH reached 7. The chemical reaction of the activation process with KOH has already been suggested: $6\text{KOH} + \text{C} \leftrightarrow 2\text{K} + 3\text{H}_2 + 2\text{K}_2\text{CO}_3$.^{15, 16}

2. Experimental methods

2.1 Synthesis of 3D crumpled structure a-NSrGO

Graphene oxide (GO) was prepared by a modified Hummer's method from natural graphite using sulfuric acid, potassium permanganate, and sodium nitrate.³ We followed our procedure, which has been described previously, to fabricate the NSGO and NSrGO powders.¹⁴ For an activation process, the 200 mg of NSrGO and 40 mL of a 7 M KOH solution were stirred for 4 h and left to stand for 20 h. The wetted NSrGO was filtered to remove any extra KOH solution, and then the filter cake was dried in a vacuum oven for one day. The dry mixture (200 mg) was placed on an ceramic boat and heated at 800°C (5°C min^{-1}) for 1 h in a ceramic tube furnace. After cooling under vacuum, the sample was repeatedly washed with trice-distilled water until the pH reached 7. The washed sample was heated again at 800°C (5°C min^{-1}) for 2 h to fully dehydrate the material. Finally, 80 mg of a-NSrGO was obtained; the yield was about 40%.

2.2 Materials characterization

Structural characterizations were performed using a JEOL JSM-7404F field emission scanning electron microscope (SEM) operating at 15 kV and a JEOL JEM-2100F transmission electron microscope (TEM). The X-ray photoelectron spectroscopy (XPS) measurements were performed on a Thermo VG Microtech ESCA 2000 with a monochromatic Al-K α X-ray source at 100 W. Raman spectra were recorded on a WITEC alpha300 with a 532 nm excitation wavelength. The Brunauer-Emmett-Teller (BET) theory for specific surface area was measured by BELSORP-max.

2.3 Fabrication of supercapacitors

Supercapacitors using NSrGO and a-NSrGO were fabricated in a symmetrical two electrode cell with 1 M TEABF₄ in a PC organic electrolyte. Al foil was used as the current collector. To prepare the electrode material slurries, 10 wt% polyvinylidene fluoride (PVDF) was added to NSrGO and a-NSrGO as a binder. These slurries were then mixed with a mortar and a ball-mill. The slurries were loaded onto the Al foil by the bar coating method and dried overnight in a vacuum oven at 80°C . Then, the dried samples were punched with 14Φ to fabricate the coin cells. The electrolyte and coin cells were fabricated in a

glove box with less than 1 ppm of moisture and oxygen. During coin cell fabrication, Celgard® 3501 was used as a separator between the electrode materials that were loaded into the current collectors. The total mass of the loaded materials in the two electrodes in the coin cell was 2.45 mg for NSrGO and 1.4 mg for a-NSrGO.

2.4 Electrochemical characterization

Cyclic voltammetry, galvanometric charge-discharge curves, and electrochemical impedance spectra over a frequency range of 0.01 Hz - 100 kHz with amplitude of 10 mV were obtained using a CHI660c electrochemical workstation. The specific capacitance (C_s) was calculated from the galvanometric charge-discharge curves. The following formula was used: $C_s = 4I/(m\Delta V/\Delta t)$, where, I is the constant current, m the total mass of both electrodes, and $\Delta V/\Delta t$ is calculated from the slope obtained by fitting a straight line to the discharge curve. The multiplier 4 adjusts the specific capacitance of the cell and the combined mass of the two electrodes to the capacitance and mass of a single electrode.

The evolution of the changes in the real (C') and imaginary (C'') parts of the capacitance versus frequency were plotted from the following equations: $C'(\omega) = -Z''(\omega)/\omega|Z(\omega)|^2$ and $C''(\omega) = Z'(\omega)/\omega|Z(\omega)|^2$, where, ω is the pulsation, $C'(\omega)$ is the real part of the capacitance, $C''(\omega)$ is the imaginary part of the capacitance, $Z(\omega)$ is the electrochemical impedance, and $Z'(\omega)$ and $Z''(\omega)$ are the real and imaginary parts of the impedance, respectively, defined as $Z'^2 + Z''^2 = |Z(\omega)|^2$.

The energy density and power density of the electrodes were calculated using the following equations: $E = (1/2 \times 1000/3600) \times C_s (\Delta V)^2$ and $P = (V_{\max} - V_{\text{drop}})^2/4(R_{\text{ESR}}m)$, where C_s (F/g) is the specific capacitance of the electrode, ΔV (V) is the potential range, E (Wh kg⁻¹) is the energy density, P (W kg⁻¹) is the power density, m (g) is the weight of electrode materials (two electrodes), and the effective series resistance (ESR) is estimated by using the voltage drop at the beginning of the discharge (V_{drop}) at a certain constant current I_{cons} (A) with following formula: $R_{\text{ESR}} = V_{\text{drop}} / (2I_{\text{cons}})$

3. Results and discussion

3.1 Morphological and structural characterization

Unlike common GO sheets, our NSGO has a crumpled 3D structure, as shown in Fig. S1.† Moreover, the NSrGO and a-NSrGO also maintain their unique structure after thermal reduction and chemical activation processes. To confirm the morphology and nanostructure, the NSrGO and a-NSrGO are characterized by scanning electron microscopy (SEM) and high-resolution transmission electron microscopy (HR-TEM). Fig. 2a-b show SEM images of the crumpled 3D structure of the NSrGO, which is visible even at high magnification. The HR-TEM images (Fig. 2c and Fig. S2a-c)† show detailed structural properties with a porous 3D structure. Although the a-NSrGO is treated by a chemical activation process, the SEM images show its unique structure (Fig. 2d-e). In the HR-TEM images of Fig. 2f and Fig. S2d-f)†, the a-NSrGO shows a more distinctive structure, with a crumpled 3D structure and many

holes (white circles in the HR-TEM images). The holes on a-NSrGO clearly indicate etching from the KOH activation process, indicating the presence of meso- and micropores in the porous materials.¹⁷ Finally, the a-NSrGO got useful micropore and an advantageous structure to EDLC mechanism, indicating easily accessible for electrolyte ions.

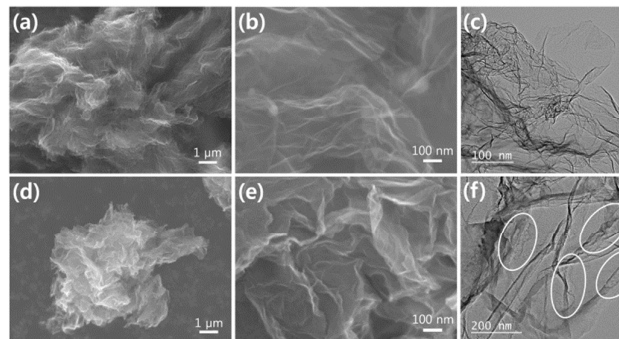


Fig. 2 The scanning electron microscopy (SEM) and high-resolution transmission electron microscopy (HR-TEM) images. (a-b): SEM images of NSrGO, (c): HR-TEM image of NSrGO, (d-e): SEM images of a-NSrGO, and (f): HR-TEM image of a-NSrGO. The SEM images of a-NSrGO show that the crumpled 3D structure is maintained after the chemical activation process. The white circles in the HR-TEM indicate the details of etched holes.

Raman spectroscopy confirmed the synthesis and structural characterization of a-NSrGO, as shown in Fig. 3a. The D bands of a-NSrGO appeared at 1349 cm⁻¹. The D band is due to the A_{1g} symmetry mode caused by breathing vibrations of six-member sp² carbon rings, and only becomes active in the presence of disorder.¹⁸ Additionally, the G bands of a-NSrGO were shown at 1583 cm⁻¹. The G band has E_{2g} symmetry, which involves the in-plane bond-stretching motion of pairs of carbon sp² atoms. This band does not require the presence of six-member rings; it occurs at all sp² sites as opposed to only those in the rings.¹⁹ The integrated D band to G band ratio (I_D/I_G) slightly increases from 1.02 in NSrGO to 1.20 in a-NSrGO due to the etching during the activation process (Fig. S3)†.

The a-NSrGO is also characterized with X-ray photoelectron spectroscopy in order to determine its structure (Fig. 3b). Primary C1s peaks appear at binding energies of 283.1 eV and 284.5 eV, which are assigned to sp² carbon bonds (C-C/C=C). There are other weak peaks at 285.7 eV, 287.1 eV, and 288.3 eV, which can be identified as the sp³ carbon bonds of the hydroxyl carbon peak (C-O), carbonyl peak (C=O), and carboxyl peak (C(O)O), respectively. This indicates that the a-NSrGO is dominated by sp² conjugated carbon. Furthermore, the C/O ratio was 15.11, which means that the obtained a-NSrGO is mainly composed of carbon atoms. The XPS data of GO and NSrGO are shown in Fig. S4.† Due to the presence of oxygen functional groups, the GO has a relatively strong peak at 287.1 eV compared to the carbonyl (C=O) sp³ carbon bond. However, the NSrGO shows a strong peak (similar to the a-NSrGO), indicating that the NSrGO is composed of carbon atoms and that the a-NSrGO also maintains a carbon-dominant composition despite the KOH activation process.

The porosity is analyzed by N_2 gas adsorption-desorption measurements with advanced methods based on Brunauer-Emmett-Teller (BET) theory for specific surface area, the Barrett-Joyner-Halenda (BJH) method for wide pore distribution, and the Horvath-Kawazoe (HK) method for sub-nanopores (pore width < 1 nm). The HK method is capable of generating model isotherms more efficiently than density functional theory (DFT) to characterize the pore size distribution of microporous materials.²⁰ Fig. 3c shows N_2 sorption isotherms with a pronounced hysteresis in the P/P_0 range (0.45 to 1.0), indicating the presence of a large number of mesopores in a-NSrGO.²¹ The BET calculation implied that the specific surface area of a-NSrGO is $999.75 \text{ m}^2 \text{ g}^{-1}$, which is higher than that of KOH-untreated NSrGO ($670.65 \text{ m}^2 \text{ g}^{-1}$). In addition, the total pore volume of a-NSrGO ($5.03 \text{ cm}^3 \text{ g}^{-1}$) is also much higher than that of the untreated NSrGO ($4.11 \text{ cm}^3 \text{ g}^{-1}$).¹⁴ Although the a-NSrGO has higher total pore volume, it shows lower volume than the NSrGO at same weights (Fig. S5†). Therefore the a-NSrGO has high packing density, which means that it can show higher performance aspect of volumetric capacitance. The plot of the BJH method (blue line in Fig. 3d) shows the wide pore size distribution of a-NSrGO (from mesopore to macropore), verifying that the maintained crumple structure of a-NSrGO can provide effective diffusion pathways to the electrolyte ions for entrance role of micropores. Furthermore, the HK plot (red line in Fig. 3d) shows the sub-nanopores (micropores) of a-NSrGO, where the main pore width is between 0.61 and 0.71 nm, and a wide range of pores from mesopores to macropores. The electrical conductivity of NSrGO and a-NSrGO were also characterized to clearly compare aspect of material performance. Although the NSrGO and a-NSrGO did not include sub-conductive materials such as carbon black, the NSrGO and a-NSrGO shows high electrical conductivity as 1209 S m^{-1} and 1202 S m^{-1} , respectively. More importantly, the a-NSrGO still maintained its high electrical conductivity after KOH activation process (Table S1†). As a result, the crumpled and etched pores of a-NSrGO allow for the easy accessibility of electrolyte ions into the macropores, mesopores, and sub-nanopores.

3.2 Electrochemical characterizations

The energy storage effect of various pore size distributions from macro- to micropores of a-NSrGO was characterized by electrochemical measurements. To prepare a full packaged coin cell type supercapacitor, a slurry mixture of a-NSrGO and 10 wt% polyvinylidene fluoride (PVDF) (as a binder) was coated on an Al current collector and then completely dried. The cell was fabricated with 1 M tetraethylammoniumtetrafluoroborate (TEABF_4) in a propylene carbonate (PC) organic electrolyte (the a-NSrGO loading mass of both electrodes was 1.4 mg). Cyclic voltammetry (CV) was first used to determine the capacitive performance of a-NSrGO (Fig. 4a). The CV curves showed nearly rectangular shapes, even at different scan rates ($10\text{--}100 \text{ mV s}^{-1}$), indicating ideal supercapacitor performance during the charge-discharge process. Since the wide pore distribution and high SSA of a-NSrGO allow for the fast diffusion of electrolyte ions in the electrode material, the CV

curves can maintain their fully-rectangular shape regardless of the scan rate. The specific capacitance of the organic electrolyte (using PC) during discharge at 10 mV s^{-1} was about 110 F g^{-1} in the range from 2.5 V to 0 V (i.e., fully discharged). The fully-symmetric galvanostatic charge-discharge curves of a-NSrGO were observed at current densities of 0.5, 1, 2, and 5 A g^{-1} (Fig. 4b), verifying that there was non-faradaic current for just the electric double layer capacitor process. The specific capacitance was 105.26 F g^{-1} , as calculated from the discharge curve at a current density of 0.5 A g^{-1} . Moreover, an IR drop was not observed at the beginning of the discharge curves, suggesting a very low ESR in a-NSrGO. In addition, the capacitance retention of a-NSrGO at a current density of 5 A g^{-1} for 10,000 cycles is shown in Fig. 4c. The 88.4% of the capacitance was kept and the rectangular CV shape was maintained after 10,000 cycles.

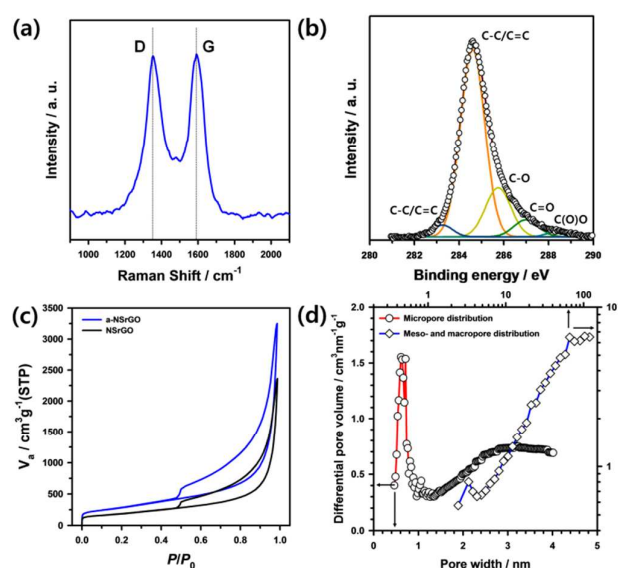


Fig. 3 (a) Raman spectra of a-NSrGO. (b) X-ray photoelectron microscopy (XPS) C1s peak analysis of a-NSrGO. (c) The N_2 sorption isotherm comparison of a-NSrGO with untreated-KOH NSrGO. (d) The pore size distribution for N_2 (calculated by the HK method). The red line and blue line indicate micropore (main pore width is 0.61~0.71 nm) and meso- to macropore (larger than micropores) distributions, respectively.

To further confirm the supercapacitor behavior, electrochemical impedance spectroscopy (EIS) measurements were performed in the frequency range from 100 kHz to 10 mHz with an amplitude of 10 mV AC. Fig. S5† shows the Nyquist plot of a-NSrGO. The plot features a vertical curve, indicating the nearly-capacitive performance of the cell. The inset of Fig. S6† is a magnified view of the high frequency range. A Nyquist plot for an electric double layer capacitor is analyzed by looking at the high frequency semicircle, which is caused by the effective series resistance (R_s). This is attributed to the ionic conductivity between the electrode materials and electrolyte.²² The a-NSrGO showed very low R_s (1.76Ω), representing the low intrinsic internal resistance of the electrode

materials and electrolyte of the supercapacitor cells.²³⁻²⁵ A transition between the RC semicircle and the migration of electrolyte was observed at a frequency of 146 Hz, which corresponds to a charge transfer resistance (R_{CT}) of 14.83 Ω . The KOH-untreated NSrGO, used as a control, was also characterized by electrochemical measurements for comparison the a-NSrGO. The electrochemical information of the NSrGO electrode is also shown in Fig. S7 and S8.† Although the NSrGO showed similar to a-NSrGO a rectangular shape in its CV and a symmetric triangle shape in its galvanostatic charge-discharge curves, the a-NSrGO (in comparison with the NSrGO) showed a larger area in its CV curve and a longer discharge time (124.7 s at a current density of 0.5 A g⁻¹) in its galvanostatic charge-discharge curves, indicating that the a-NSrGO exhibited superior energy storage performance.

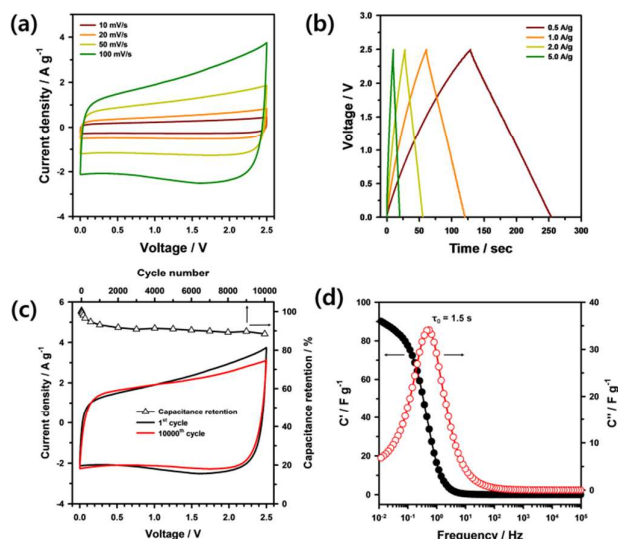


Fig. 4 The electrochemical behaviors of a-NSrGO in a PC-based, 1 M TEABF₄ organic electrolyte. (a) Cyclic voltammetry (CV) curves at various scan rates. (b) Galvanostatic charge-discharge curves at various current densities. (c) The cyclic test at a current density of 5 A g⁻¹ for 10,000 cycles. The capacitance retention (black triangle line) and the CV curve comparison between the initial cycle (black line) and after 10,000 cycles are shown. (d) Evolution of the real (C' , black circle line) and imaginary (C'' , red circle line) parts of the capacitance of the supercapacitor based on a-NSrGO. A low relaxation time constant ($\tau_0 = 1.5$ s) was obtained, despite the fact that a PC-based organic electrolyte was used.

To consider the supercapacitor as a whole by using the impedance data, Fig. 4d presents the real part of the capacitance (C') change (filled circle, black line) and the imaginary part of the capacitance (C'') change (open circle, red line) versus frequency for a-NSrGO. When the frequency decreases, the C' significantly increases and then tends to be less frequency-dependent; this is related to the electrode structure and interface between the electrode and electrolyte.^{26, 27} However, the C'' curve shows a peak at frequency f_0 , describing the dielectric relaxation time constant as $\tau_0 = 1/f_0 = 1.5$ s. τ_0 is the minimum

time needed to discharge all of the energy from the cell with an efficiency greater than 50%.²⁸ Surprisingly, the a-NSrGO shows a short relaxation time in spite of using a PC-based organic electrolyte, which has a higher viscosity and dielectric constant than an acetonitrile (ACN) electrolyte (activated carbon supercapacitor using PC for $\tau_0 = 48$ s and ACN for $\tau_0 = 10$ s).²⁶ Commonly, PC electrolyte-based cells are more attractive compared to ACN-based cells due to their stable, non-toxic, and non-volatile properties, especially for commercial applications, although PC-based cells typically show slower charging-discharging performance than the ACN-based cells.²⁹ Finally, in Fig. 5a, the rectangular CV area of a-NSrGO is two times larger than that of NSrGO, verifying the fact that the specific capacitance of a-NSrGO is two times higher than NSrGO for energy storage performance in PC-based cells and operate two times faster up to same capacitance. Furthermore, due to its short relaxation time (1.5 s), the a-NSrGO also demonstrates high power performance.

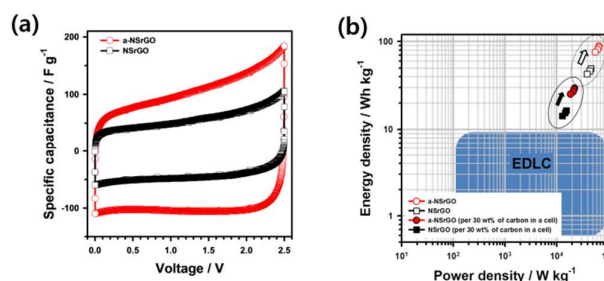


Fig. 5 (a) The rectangular CV curves of a-NSrGO compared with NSrGO (as a control) at a scan rate of 10 mV s⁻¹, showing the higher energy storage performance of a-NSrGO. (b) The Ragone plot of a-NSrGO and NSrGO showing energy density and power density at PC-based 1 M TEABF₄ organic electrolyte system (black dotted circle line). The normalized energy density and power density using the total mass of fully packaged cell (30 wt%) were also indicated (black solid circle line).

In the Ragone plot (Fig. 5b), the maximum energy density of 91.13 Wh kg⁻¹ for a-NSrGO was estimated in full packaged coin cell, which is much higher than the maximum energy density of 49.31 Wh kg⁻¹ for NSrGO. And the maximum power density of a-NSrGO (66684.73 W kg⁻¹) also showed higher value than that of NSrGO (46512.73 W kg⁻¹). Supercapacitors are in that they contain current collectors, electrolyte, separator, binder, and packing. Because the carbon weight accounts for about 30% of total mass (30 wt%) of packaged commercial supercapacitors, a factor of 1/3 to 1/4 is frequently used to extrapolate the energy density and power density of the device from performance of materials.³⁰ To extrapolate the energy density and power density values in full packaged cell, we assumed the carbon material weights account for about 30 wt% of total mass of the packaged commercial cell.^{21, 30} The normalized maximum energy density and power density of a-NSrGO were 30.38 Wh kg⁻¹ and 22228.24 W kg⁻¹, respectively.

These are much higher than that of the current state-of-the-art commercial supercapacitors.³¹ As a result, the superior performances of the a-NSrGO including high pore volume, SSA, and electrical conductivity can synthetically provide high power performance as well as high energy storage effects, which were higher than previously reported energy and power density values of crumpled structure carbon materials (Table S2†).

4. Conclusions

In summary, we developed activated, porous, and crumpled 3D graphene (a-NSrGO) via simple KOH activation of NSrGO to provide high SSA and electrical conductivity electrodes that enable fast diffusion of the electrolyte. This combination of properties leads to high power performance in supercapacitors. The a-NSrGO was characterized by Raman and XPS to show the properties of graphene with a crumpled structure, many holes, and a wide pore size distribution (from macropores to micropores). BET showed that the a-NSrGO had high specific surface area ($999.75 \text{ m}^2 \text{ g}^{-1}$) and high total pore volume ($5.03 \text{ cm}^3 \text{ g}^{-1}$). The wide range of the pore size distribution is essential for creating energy storage space for electrolyte ions that use narrow micropores for fast diffusion. Furthermore, the a-NSrGO also shows maintenance of high electrical conductivity as 1202 S m^{-1} , leading power performance. As a result, during supercapacitor application with a PC-based organic electrolyte with 1 M TEABF_4 , the specific capacitance of a-NSrGO was 105.26 F g^{-1} at a current density of 0.5 A g^{-1} . The EIS results of the supercapacitor cell showed low resistance: R_s of 1.76Ω and R_{CT} of 14.83Ω . Furthermore, its relaxation time (τ_0) was 1.5 s , indicating a very short time for high power performance and a fast diffusion rate of the electrolyte ions. Finally, the maximum energy density of 91.13 Wh kg^{-1} and power density of $66684.73 \text{ W kg}^{-1}$ were estimated in full packaged coin cell. Based on these superior properties, the a-NSrGO has a strong potential to be utilized in industrial energy storage applications such as Li-ion batteries, fuel cells, and energy conversion systems.

Acknowledgements

This work was supported by the Institute for Basic Science (IBS-R011-D1) and partially by ISTK (Grant CAP-13-2-ETRI).

References

- X. Huang, X. Y. Qi, F. Boey and H. Zhang, *Chem Soc Rev*, 2012, **41**, 666-686.
- X. Huang, Z. Y. Yin, S. X. Wu, X. Y. Qi, Q. Y. He, Q. C. Zhang, Q. Y. Yan, F. Boey and H. Zhang, *Small*, 2011, **7**, 1876-1902.
- I. K. Moon, J. Lee, R. S. Ruoff and H. Lee, *Nat Commun*, 2010, **1**.
- M. D. Stoller, S. J. Park, Y. W. Zhu, J. H. An and R. S. Ruoff, *Nano Lett*, 2008, **8**, 3498-3502.
- L. L. Zhang, R. Zhou and X. S. Zhao, *J Mater Chem*, 2010, **20**, 5983-5992.

- K. S. Novoselov, V. I. Fal'ko, L. Colombo, P. R. Gellert, M. G. Schwab and K. Kim, *Nature*, 2012, **490**, 192-200.
- L. L. Zhang and X. S. Zhao, *Chem Soc Rev*, 2009, **38**, 2520-2531.
- P. Simon and Y. Gogotsi, *Nat Mater*, 2008, **7**, 845-854.
- M. Segal, *Nat Nanotechnol*, 2009, **4**, 611-613.
- L. Zhang, F. Zhang, X. Yang, G. K. Long, Y. P. Wu, T. F. Zhang, K. Leng, Y. Huang, Y. F. Ma, A. Yu and Y. S. Chen, *Sci Rep-Uk*, 2013, **3**.
- J. Chmiola, C. Largeot, P. L. Taberna, P. Simon and Y. Gogotsi, *Angew. Chem. Int. Ed.*, 2008, **47**, 3392-3395.
- J. Chmiola, G. Yushin, Y. Gogotsi, C. Portet, P. Simon and P. L. Taberna, *Science*, 2006, **313**, 1760-1763.
- Y. Gogotsi, A. Nikitin, H. H. Ye, W. Zhou, J. E. Fischer, B. Yi, H. C. Foley and M. W. Barsoum, *Nat Mater*, 2003, **2**, 591-594.
- Y. Yoon, K. Lee, C. Baik, H. Yoo, M. Min, Y. Park, S. M. Lee and H. Lee, *Adv. Mater.*, 2013, **25**, 4437-4444.
- Y. W. Zhu, S. Murali, M. D. Stoller, K. J. Ganesh, W. W. Cai, P. J. Ferreira, A. Pirkle, R. M. Wallace, K. A. Cychosz, M. Thommes, D. Su, E. A. Stach and R. S. Ruoff, *Science*, 2011, **332**, 1537-1541.
- C. Portet, M. A. Lillo-Rodenas, A. Linares-Solano and Y. Gogotsi, *Phys Chem Chem Phys*, 2009, **11**, 4943-4945.
- B. Ding, C. Z. Yuan, L. F. Shen, G. Y. Xu, P. Nie, Q. X. Lai and X. G. Zhang, *J Mater Chem A*, 2013, **1**, 1096-1101.
- S. Niyogi, E. Bekyarova, M. E. Itkis, H. Zhang, K. Shepperd, J. Hicks, M. Sprinkle, C. Berger, C. N. Lau, W. A. Deheer, E. H. Conrad and R. C. Haddon, *Nano Lett*, 2010, **10**, 4061-4066.
- A. C. Ferrari and J. Robertson, *Phys Rev B*, 2000, **61**, 14095-14107.
- R. J. Dombrowski and C. M. Lastoskie, *Stud Surf Sci Catal*, 2002, **144**, 99-106.
- T. Kim, G. Jung, S. Yoo, K. S. Suh and R. S. Ruoff, *ACS Nano*, 2013, **7**, 6899-6905.
- Y. Yoon, K. Lee, S. Kwon, S. Seo, H. Yoo, S. Kim, Y. Shin, Y. Park, D. Kim, J. Y. Choi and H. Lee, *ACS Nano*, 2014, **8**, 4580-4590.
- S. B. Yang, X. L. Wu, C. L. Chen, H. L. Dong, W. P. Hu and X. K. Wang, *Chem. Commun.*, 2012, **48**, 2773-2775.
- E. Frackowiak and F. Beguin, *Carbon*, 2001, **39**, 937-950.
- C. Portet, P. L. Taberna, P. Simon and C. Laberty-Robert, *Electrochim. Acta*, 2004, **49**, 905-912.
- P. L. Taberna, P. Simon and J. F. Fauvarque, *J Electrochem Soc*, 2003, **150**, A292-A300.
- W. P. Si, C. L. Yan, Y. Chen, S. Oswald, L. Y. Han and O. G. Schmidt, *Energ Environ Sci*, 2013, **6**, 3218-3223.
- D. Pech, M. Brunet, H. Durou, P. H. Huang, V. Mochalin, Y. Gogotsi, P. L. Taberna and P. Simon, *Nat. Nanotechnol.*, 2010, **5**, 651-654.
- P. W. Ruch, D. Cericola, A. Foelske, R. Kotz and A. Wokaun, *Electrochim Acta*, 2010, **55**, 2352-2357.
- Y. Gogotsi and P. Simon, *Science*, 2011, **334**, 917-918.
- A. R. D. Burke, *Electrochim. Acta*, 2007, **53**, 1083-1091.